# Bound-bound transitions in hydrogenlike ions in Debye plasmas

Y. Y. Qi,[1,2] J. G. Wang,[2] and R. K. Janev[3]
[1]*School of Electrical Engineering, Jiaxing University, Jiaxing 314001, China*
[2]*Laboratory of Computational Physics, Institute of Applied Physics and Computational Mathematics, P.O. Box 8009-26, Beijing 100088, China*
[3]*Macedonian Academy of Sciences and Arts, P.O. Box, 428, 1000 Skopje, Macedonia*
(Received 14 October 2008; published 31 December 2008)

Plasma screening effects on the properties of bound-bound transitions of hydrogenlike ions imbedded in Debye plasmas are investigated. The electron eigenenergies and wave functions are determined by numerically solving the scaled Schrödinger equation with a Debye potential by the fourth-order symplectic integration scheme. The scaled spectral properties of hydrogenlike ions in the plasma, including the transition frequencies, absorption oscillator strengths, radiative transition probabilities, as well as the line intensities of the Lyman and Balmer series, are presented for a wide range of plasma screening parameters. While for the $\Delta n \neq 0$ transitions the oscillator strengths and spectral line intensities decrease with increasing the plasma screening, those for the $\Delta n=0$ transitions rapidly increase. The lines associated with the $\Delta n \neq 0$ transitions are redshifted, whereas those for $\Delta n=0$ transitions are blueshifted. Comparison of present results with those of other authors, when available, is made. The results reported here should be useful in the interpretation of spectral properties of hydrogenlike ions in laboratory and astrophysical Debye plasmas.

DOI: 10.1103/PhysRevA.78.062511 PACS number(s): 32.70.Cs

## I. INTRODUCTION

The effects of screened Coulomb interaction between charged particles in hot, dense plasmas on the atomic structure and collision properties have been subject to extensive studies in the last 30–40 years (see, e.g., [1,2], and references therein). These studies have been motivated mainly by the research in laser produced plasmas, euv and x-ray laser development, inertial confinement fusion, and astrophysics (stellar atmospheres and interiors). The densities ($n$) and temperatures ($T$) in these plasmas span the ranges $n \sim 10^{15}-10^{18}$ cm$^{-3}$, $T \sim 0.5-5$ eV (stellar atmospheres), $n \sim 10^{19}-10^{21}$ cm$^{-3}$, $T \sim 50-300$ eV (laser plasmas) and $n \sim 10^{22}-10^{26}$ cm$^{-3}$, $T \sim 0.5-10$ keV (inertial confinement fusion plasmas). The Coulomb interaction screening in these plasmas is a collective effect of the correlated many-particle interactions, and in the lowest particle correlation order (pairwise correlations) it reduces to the Debye-Hückel potential (for the interaction of an ion of charge $Z$ with an electron) [1,2]

$$V(r) = -\frac{Ze^2}{r}\exp\left(-\frac{r}{D}\right), \tag{1}$$

where $D=(k_B T_e/4\pi e^2 n_e)^{1/2}$ is the Debye screening length, $T_e$ and $n_e$ are the plasma electron temperature and density, respectively, and $k_B$ is the Boltzmann constant. The representation of charged particle interaction in a plasma by the potential (1) is adequate only if the Coulomb coupling parameter $\Gamma=e^2/(ak_B T_e)$ and plasma nonideality parameter $\gamma=e^2/(Dk_B T_e)$ satisfy the conditions $\Gamma \leqslant 1$, $\gamma \ll 1$, where $a=[3/(4\pi n_e)]^{1/3}$ is the average interparticle distance. There is, however, a wide class of laboratory and astrophysical plasmas in which these conditions are fulfilled (Debye plasmas). Expressions for the screened Coulomb interaction for strongly coupled and nonideal plasmas can be found elsewhere (see, e.g., [1,2]).

The purpose of the present work is to study the properties of bound-bound transitions of a hydrogenlike ion with the potential (1). Studies of this type have been performed earlier in [3–5] for a limited number of Debye lengths and have concentrated on the calculation of oscillator strengths [4,5] or radiative transition probabilities [3] only. In the present study we cover the entire range of Debye screening lengths and analyze in detail the properties of transition frequencies and spectral line intensities and shifts. Particular attention will be paid to the $\Delta n=0$ transitions whose line intensities increase (in contrast to the $\Delta n \neq 0$ transitions) with increasing the screening strength, $1/D$. The line intensities of Lyman and Balmer series will also be studied in detail, including different line intensity ratios within a given series.

Besides the intrinsic interest in the study of structure and radiative properties of atomic systems with short-range, Yukawa-type interactions, the specific motivation for the present systematic study of radiative properties of hydrogenlike ions in Debye plasmas has been the increased accuracy level of spectroscopic observations of atomic radiation from hot, dense laboratory plasmas [6–10] and the need for their proper interpretation (especially when it is used for plasma diagnostic purposes). In all these experiments the redshift of spectral lines has been clearly observed, as well as the reduction of the Lyman series to a finite number [3,4] of lines. It should be noted that in Refs. [9,10] the redshift of H Lyman series lines and the termination of the series at the Lyman-$\gamma$ line has been observed during the ablation of H-ice pellets in a thermonuclear fusion plasma, the pellet cloud providing locally the necessary high plasma density.

The paper is organized as follows. In the next section we briefly outline the theoretical method used for determination of eigenenergies and the wave functions of a hydrogenlike ion with the potential (1). In this section we also present in scaled form the results for the bound state energies as function of the scaled screening strength $\mu=1/(ZD)$, as well as the results for the transition energies between the states. In

 

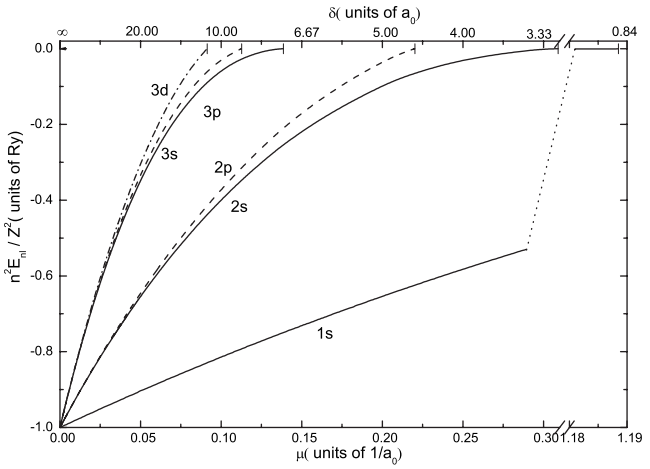


FIG. 1. Scaled energies for the six lowest states of hydrogenlike ion as function of scaled screening parameter $\mu=1/ZD$.

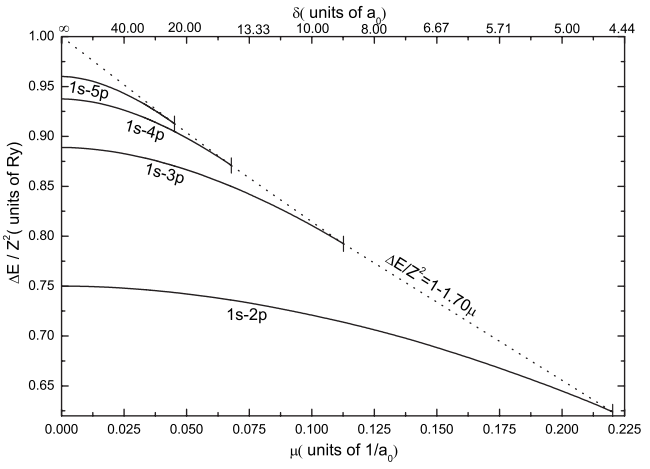


FIG. 2. Scaled energy differences between the $1s$ and $np$ ($n \leqslant 5$) states of hydrogenlike ion as function of scaled screening parameter $\mu$.

Sec. III we present in scaled form the results for the oscillator strengths, transition probabilities and lifetimes as function of the screening parameter $\mu$. In Sec. IV we discuss the properties of the spectral lines for both $\Delta n \neq 0$ and $\Delta n=0$ transitions assuming a Doppler line profile, and in Sec. V we give our conclusions.

Atomic units will be used in the remaining part of this paper, unless explicitly indicated otherwise.

## II. THEORETICAL METHOD, SCALED ENERGIES, AND WAVELENGTHS

In the nonrelativistic approximation, the radial Schrödinger equation for a hydrogenlike ion with nuclear charge $Z$ in a Debye plasma is given by

TABLE I. Values of the critical scaled screening lengths $\delta_{nl}=ZD_{nl}$ (units of $a_0$).

| | $l$ | | | | |
|---|---|---|---|---|---|
| $n$ | 0 | 1 | 2 | 3 | 4 |
| 1 | 0.8414 (0.8399)[a] | | | | |
| 2 | 3.236 (3.223) | 4.541 (4.541) | | | |
| 3 | 7.213 (7.171) | 8.875 (8.872) | 10.948 (10.947) | | |
| 4 | 12.785 (12.687) | 14.74 (14.731) | 17.215 (17.210) | 20.065 (20.068) | |
| 5 | 19.999 (19.772) | 22.149 (22.130) | 24.990 (24.985) | 28.257 (28.257) | 31.905 (31.904) |

[a]The values in parentheses are from Ref. [13].

$$\left(-\frac{d^2}{2dr^2}+\frac{l(l+1)}{2r^2}+V(r)\right)P_{nl}(r;Z,D)=E_{nl}(Z,D)P_{nl}(r;Z,D), \tag{2}$$

where $P_{nl}(r;Z,D)$ is the radial electron wave function, $n$ and $l$ are, respectively, the principal and angular quantum numbers, and the potential $V(r)$ is given by Eq. (1) (with $e^2=1$).

By making the scaling transformations

$$\rho=Zr, \quad \delta=ZD, \quad \varepsilon_{nl}(\delta)=E_{nl}(Z,D)/Z^2, \tag{3}$$

Eq. (2) is reduced to the form

$$\left(-\frac{d^2}{2d\rho^2}+\frac{l(l+1)}{2\rho^2}-\frac{\exp(-\rho/\delta)}{\rho}\right)P_{nl}(\rho;\delta)=\varepsilon_{nl}(\delta)P_{nl}(\rho;\delta). \tag{4}$$

It is obvious that the substitutions (3) conserve the normalization condition

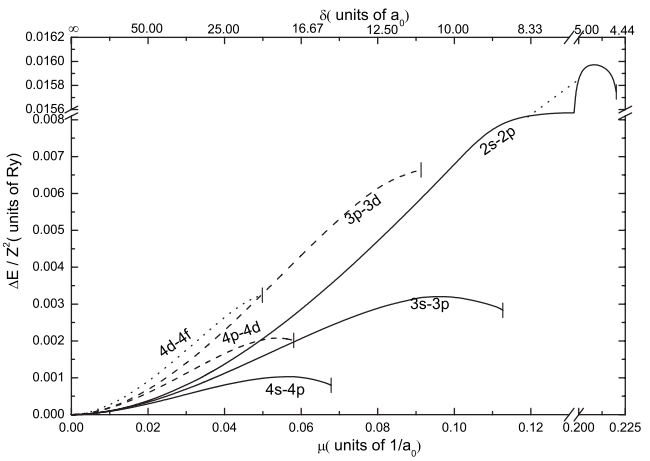


FIG. 3. Scaled transition energies for the $\Delta n=0$, $\Delta l=1$ transitions ($n=2,3,4$) as function of screening parameter $\mu$.

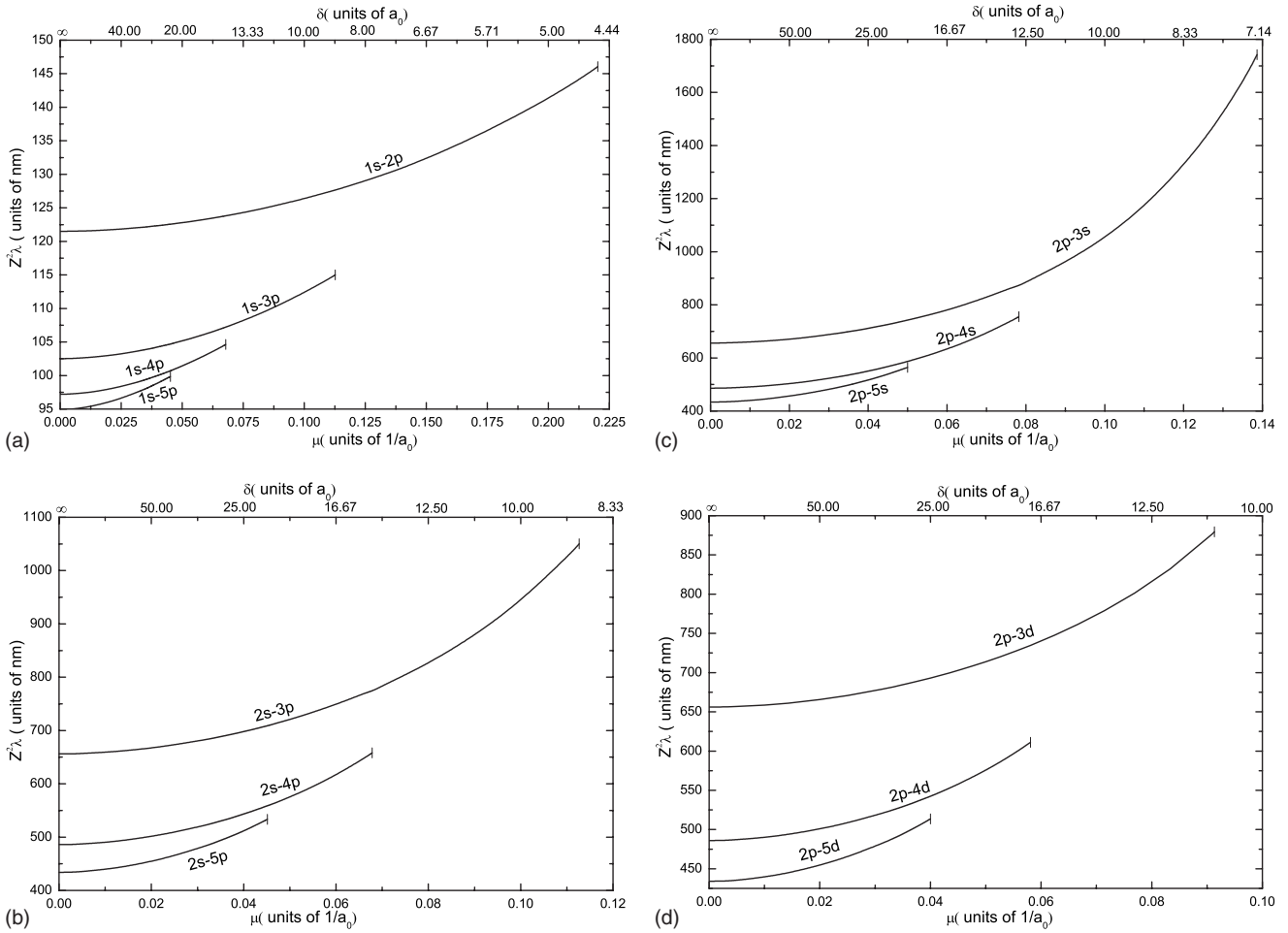


FIG. 4. Scaled wavelengths as function of screening parameter $\mu$. Panel (a), Lyman series; panels (b), (c), and (d), the three branches of the Balmer series.

$$\int_0^\infty |P_{nl}(r;Z,D)|^2 dr = \int_0^\infty |P_{nl}(\rho;\delta)|^2 d\rho = 1, \tag{5}$$

and lead to the $Z$ scaling of matrix elements

$$\langle P_{nl}(r;Z,D)|r^k|P_{n'l'}(r;Z,D)\rangle = Z^{-k}\langle P_{nl}(\rho;\delta)|\rho^k|P_{n'l'}(\rho;\delta)\rangle. \tag{6}$$

The scaled radial Schrödinger equation (4) for the discrete spectrum has been subject to solution in the past by a variety of approximate (perturbation, e.g., [11]), variational (e.g., [12], and references therein), and direct numerical integration methods (e.g., [13], and references therein). In Ref. [13] the eigenenergies of Eq. (4) for the $nl$ states with $n \leqslant 9$ were calculated in a wide range of the scaled Debye length $\delta$.

For the purposes of the present work we solve Eq. (4) in the discrete spectrum numerically, under the standard boundary conditions, by employing the fourth-order symplectic integration scheme described in Refs. [14,15]. Introducing the functions $P$ and $Q$ by the relations

$$\dot{P} = dP_{nl}(\rho;\delta)/d\rho = Q, \quad \dot{Q} = -BP, \tag{7}$$

Eq. (4) can be written in the canonical Hamiltonian form

$$\begin{pmatrix} \dot{P} \\ \dot{Q} \end{pmatrix} = \begin{pmatrix} 0 & 1 \\ -B & 0 \end{pmatrix} \begin{pmatrix} P \\ Q \end{pmatrix}, \tag{8}$$

with $B = 2\varepsilon_{nl}(\delta) + 2\exp(-\rho/\delta)/\rho - l(l+1)/\rho^2$.

The spatial variation of the solutions of Eq. (8) are symplectic, so that they can be solved numerically in a symplectic scheme for given boundary conditions. The explicit fourth-order symplectic integration scheme, with four steps within each $[\rho_n, \rho_{n+1}]$ interval, can be written as [14,15]

$$v_1 = Q^n - c_1 hB(\rho_n)P^n, \quad \mu_1 = P^n + d_1 h v_1, \quad \tau_1 = \rho_n + d_1 h,$$

$$v_2 = v_1 - c_2 hB(\tau_1)\mu_1, \quad \mu_2 = \mu_1 + d_2 h v_2, \quad \tau_2 = \tau_1 + d_2 h,$$

$$v_3 = v_2 - c_3 hB(\tau_2)\mu_2, \quad \mu_3 = \mu_2 + d_3 h v_3, \quad \tau_3 = \tau_2 + d_3 h,$$

$$Q^{n+1} = v_3 - c_4 hB(\tau_3)\mu_3, \quad P^{n+1} = \mu_3 + d_4 h v_3, \tag{9}$$

where $\alpha = (2 - 2^{1/3})^{-1}$, $\beta = 1 - 2\alpha$, $c_1 = 0$, $c_2 = \alpha$, $c_3 = \beta$, $c_4 = c_2$, and $d_1 = \alpha/2$, $d_2 = (\alpha+\beta)/2$, $d_3 = d_2$, $d_4 = d_1$.

The bound state radial wave functions $P_{nl}(\rho;\delta)$ satisfy the usual boundary conditions

$$P_{nl}(0;\delta) = 0,$$

TABLE II. Oscillator strengths for Lyman series for a number of scaled Debye lengths $\delta$ (units of $a_0$).

| | $1s$-$np$ | | | |
|---|---|---|---|---|
| $\delta$ ($a_0$) | 2 | 3 | 4 | 5 |
| $\infty$ | 0.4162 | 0.0791 | 0.0290 | 0.0139 |
| 100 | 0.4155<br>(0.416)[a] | 0.0785<br>(0.0784) | 0.02812<br>(0.0282) | 0.0130<br>(0.0130) |
| 50 | 0.4136<br>(0.410) | 0.0767<br>(0.0728) | 0.0261<br>(0.0219) | 0.0108<br>(0.00635) |
| 40 | 0.4123 | 0.0754 | 0.0247 | 0.00926 |
| 20 | 0.40175<br>(0.402)<br>[0.40165][b] | 0.06585<br>(0.0658)<br>[0.06579] | 0.01448<br>(0.0145)<br>[0.01448] | |
| 10 | 0.3630 | 0.0298 | | |
| 5 | 0.1933 | | | |

[a]Data from Ref. [4].
[b]Data from Ref. [5].

$$P_{nl}(\infty;\delta) = 0. \tag{10}$$

In the present implementation of the symplectic integrator method we have, for a given $\delta$, computed $P_{nl}(\rho)$ on the interval $[0,X]$, where $X$ is a sufficiently large point in the asymptotic region so that $P_{nl}(X)$ can be obtained from the WKB solution of Eq. (4). A linear mesh has been applied, which is similar to that adopted in Ref. [16]. The mesh is composed of $m$ blocks, and each block has $N$ equally spaced intervals. The interval $h_0$ in the first block is chosen and doubled in each successive block. The values of $m$, $N$, $h_0$ are appropriately chosen for each $nl$ subshell to ensure an accuracy of $10^{-7}$ for the eigenenergies and an accuracy of $10^{-5}$ for the wave functions.

As it is well known (see, e.g., [17]), the potential (1) that decreases with increasing $r$ faster than $-1/r^2$ supports only a finite number of bound states for any finite value of $D$. Moreover, the $l$ degeneracy of the energy levels, characteristic for the pure Coulomb potential, is lifted in the screened Coulomb potential (1). The finite number of bound states for any finite value of $D$ implies that with decreasing $D$ the electron binding energy decreases and at a certain critical value $D_{nl}$ it becomes zero. In Fig. 1 we show the scaled energies $\varepsilon_{nl}$ of the 1 s, $2l$, and $3l$ states as function of the screening parameter $\mu=1/\delta$. The figure shows that with increasing $\mu$ the scaled energies rapidly approach the continuum edge. The critical scaled Debye lengths, $\delta_{nl}=ZD_{nl}$, where $\varepsilon_{nl}(\delta_{nl})=0$, are given in Table I for all the states with $n\leqslant 5$. They are compared with the values obtained in Ref. [13]. The slight disagreement of $\delta_{nl}$ values for the low $l$ substates in the two calculations reflects the fact that close to the continuum edge the integration step in the calculations was slightly different. This, however, does not affect the energy values outside the immediate vicinity of the continuum edge. For the purposes of the present paper, the agreement of the two data sets can be considered quite adequate.

In Fig. 2 we present the scaled energy differences $\Delta\varepsilon_{np,1s}=(E_{np}-E_{1s})/Z^2$ between the $1s$ and $np(n\leqslant 5)$ states (the transition frequencies of the Lyman series) as function of the scaled screening parameter $\mu$. The figure shows that with increasing the plasma screening, the transition frequencies of the Lyman series rapidly decrease. For a given $np$ state, the function $\Delta\varepsilon_{np,1s}(\mu)$ terminates at $\mu_{np}=1/\delta_{np}$, the critical screening parameter when the energy of $np$ state enters the continuum. It is interesting to observe that the end values, $\Delta\varepsilon^c_{np,1s}$, of transition energies of the Lyman series, as function of $\mu$, lie on the line $\Delta\varepsilon^c_{np,1s}[\mathrm{Ry}]=1-1.70\mu_{np}$. (Obviously, for $\mu\to 0$ and $n\to\infty$, $\Delta\varepsilon^c_{np,1s}[\mathrm{Ry}]=1$.)

It should be noted that due to the lifting of the energy degeneracy of the $n=2$ state in the screened Coulomb potential (1), the traditional Balmer series of hydrogenlike ions is now split into three branches of dipole-allowed transitions: $2s-np$, $2p-ns$, and $2p-nd$, where $n\geqslant 3$. The higher series

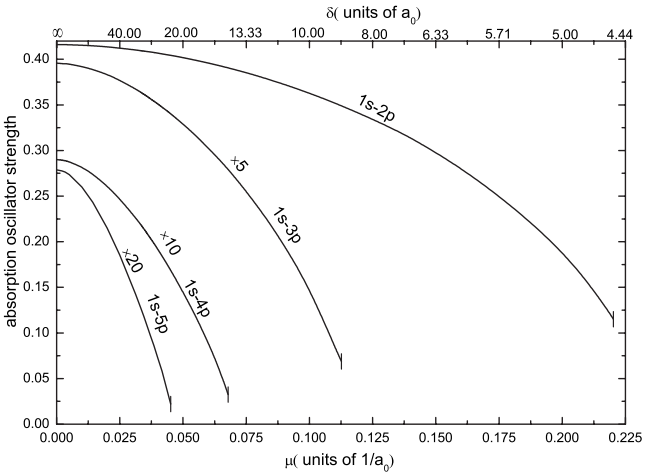


FIG. 5. Dependence of absorption oscillator strengths $f_{1s,np}$ on the screening parameter $\mu$.

TABLE III. Oscillator strengths for the three branches of Balmer series for a number of scaled Debye lengths $\delta$ (units of $a_0$).

| | $2l$-$nl'$ | | | | | | | | |
|---|---|---|---|---|---|---|---|---|---|
| $\delta$ ($a_0$) | 2$s$-3$p$ | 2$s$-4$p$ | 2$s$-5$p$ | 2$p$-3$s$ | 2$p$-4$s$ | 2$p$-5$s$ | 2$p$-3$d$ | 2$p$-4$d$ | 2$p$-5$d$ |
| $\infty$ | 0.435 | 0.103 | 0.0419 | 0.0136 | 0.00304 | 0.00121 | 0.696 | 0.122 | 0.0444 |
| 500 | 0.435 | 0.103 | 0.0418 | 0.0136 | 0.00304 | 0.00121 | 0.696 | 0.122 | 0.0443 |
| 100 | 0.431 | 0.101 | 0.0396 | 0.0136 | 0.00299 | 0.00115 | 0.692 | 0.120 | 0.0424 |
| 50 | 0.422 | 0.0950 | 0.0340 | 0.0135 | 0.00287 | 0.00101 | 0.682 | 0.115 | 0.0372 |
| 40 | 0.416 | 0.0910 | 0.0300 | 0.0134 | 0.00278 | 9.03E−4 | 0.674 | 0.112 | 0.0332 |
| 25 | 0.390 | 0.0744 | 0.0130 | 0.0132 | 0.00240 | 4.54E−4 | 0.643 | 0.0941 | |
| 20 | 0.367 | 0.0587 | | 0.0129 | 0.00202 | | 0.612 | | |
| 10 | 0.171 | | | 0.0102 | | | | | |

of hydrogenlike ions in the plasma screening case are also similarly split into $2n_0-1$ branches, where $n_0$ is the principal quantum number of lower state. The transition energies of all "daughter" series of $\Delta n \neq 0$, $\Delta l = \pm 1$ transitions, as function of the screening parameter $\mu$, also decrease with increasing $\mu$.

The situation, however, is quite different with the behavior of the transition energies as function of the interaction screening for the $\Delta n=0$, $\Delta l = \pm 1$ transitions. Figure 3 shows the $\mu$ dependence of transition energies for the $\Delta n=0$, $\Delta l=1$ transitions for $n=2,3,4$. It can be seen that with increasing $\mu$ the transition energy $\Delta\varepsilon_{nl,nl+1}(\mu)$ between these states increases, but with the approach of $\mu$ to the critical value $\mu_{n,l+1}$ the observed increase becomes increasingly weaker and the transition energy may even start to decrease (as in the case of $ns$-$np$ and 4$p$-4$d$ transitions in Fig. 3). This is due to the fact that the gradient of the energy level $\varepsilon_{nl}(\mu)$ rapidly decreases when the energy level approaches the continuum edge and because, for a given $n$, $\mu_{n,l+1} < \mu_{n,l}$.

In Fig. 4 we show the $Z$-scaled wavelengths for the Lyman series [panel (a)] and for the three branches of the Balmer series [panels (b), (c), and (d)] as a function of the screening parameter $\mu$. For a given transition the corresponding wavelengths rapidly increase with increasing the screening and terminate at the critical value $\mu_{n,l}$ of the corresponding upper state. In accordance with Fig. 3, the wavelengths of the $\Delta n=0$, $\Delta l=1$ transitions, however, decrease with increasing $\mu$ (except when $\mu$ is close to $\mu_{n,l}$).

## III. OSCILLATOR STRENGTHS, RADIATIVE TRANSITION PROBABILITIES AND LIFETIMES OF THE STATES

The absorption oscillator strength for the transition $|nl> \rightarrow |n'l'>$ in the hydrogenlike ion with nuclear charge $Z$ in the Debye plasma with screening length $D$ is [18]

TABLE IV. Oscillator strengths for the $\Delta n=0$ ($n \leqslant 3$) transitions for a number of Debye screening lengths $\delta$ (units of $a_0$).

| | $\Delta n=0$ | | |
|---|---|---|---|
| $\delta$ ($a_0$) | 2$s$-2$p$ | 3$s$-3$p$ | 3$p$-3$d$ |
| $\infty$ | 0 | 0 | 0 |
| 500 | $3.549\times10^{-5}$ | $2.106\times10^{-4}$ | $1.764\times10^{-4}$ |
| 100 | $8.669\times10^{-4}$ | 0.00499 | 0.00418 |
| 50 | 0.00336 | 0.0188 | 0.0159 |
| 40 | 0.00518 | 0.0287 | 0.0245 |
| 25 | 0.0128 | 0.0696 | 0.0618 |
| 20 | 0.0196 | 0.107 | 0.0981 |
| 11 | 0.0623 | 0.368 | 0.485 |
| 10 | 0.0752 | 0.470 | |
| 9 | 0.0930 | 0.626 | |
| 8 | 0.119 | | |
| 7 | 0.159 | | |
| 6 | 0.228 | | |
| 5 | 0.379 | | |

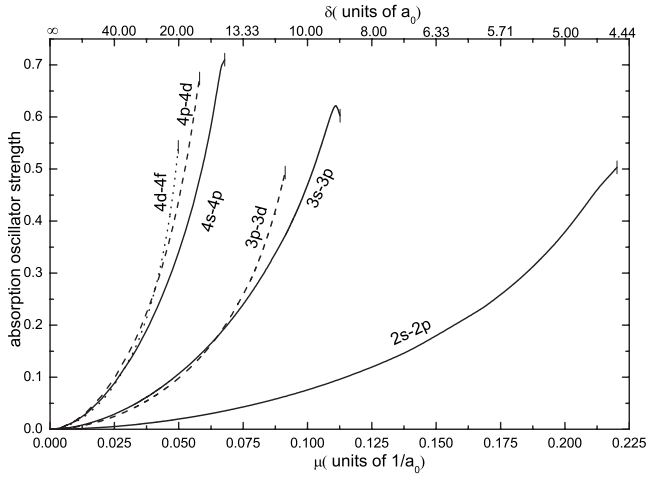


FIG. 6. Dependence of oscillator strengths for $\Delta n=0 (n \leqslant 4)$ transitions on the screening parameter $\mu$.

$$f_{nl,n'l'}(Z,D) = \frac{2[E_{n'l'}(Z,D) - E_{nl}(Z,D)]}{3(2l+1)} |\langle n'l'|r|nl\rangle|^2, \tag{11}$$

which, in view of the transformations (3) and the relation (6), takes the form

$$f_{nl,n'l'}(Z,D) = f_{nl,n'l'}(\delta) = \frac{2\omega_{nl,n'l'}}{3} \frac{(l+1)}{(2l+1)} |\langle P_{n'l'}|\rho|P_{nl}\rangle|^2, \tag{12}$$

where $\omega_{nl,n'l'}(\delta) = \varepsilon_{n'l'} - \varepsilon_{nl}$ is the transition frequency. $f_{nl,n'l'}(\delta)$ is the oscillator strength for the $|nl> \rightarrow |n'l'>$ transition in a hydrogen atom with a Debye potential having screening length $\delta$.

The spontaneous radiative decay probability $A_{n'l',nl}(Z,D)$ for the transition $|n'l'> \rightarrow |nl>$ in a hydrogenlike ion with nuclear charge $Z$ embedded in a Debye plasma with screening length $D$ can be similarly expressed in terms of the hydrogen atom radiative transition probability with a Debye potential having screening length $\delta$,

$$A_{n'l',nl}(Z,D) = Z^4 A_{n'l',nl}(\delta), \tag{13}$$

where

$$A_{n'l',nl}(\delta) = 2\frac{2l+1}{2l'+1} \alpha^3 \omega^2_{nl,n'l'}(\delta) f_{nl,n'l'}(\delta) \tag{14}$$

with $\alpha$ being the fine-structure constant.

In Table II we give the absorption oscillator strengths for the Lyman series (up to $n=5$) for a number of screening lengths $\delta$. For the value $\delta=20a_0$ they are compared with the values from Refs. [4,5], and for $\delta=50a_0$ and $\delta=100a_0$ they are compared with the values from Ref. [4]. The differences in the $f_{1s,np}(\delta)$ values reflect the accuracies of the numerical methods used for solving the radial Schrödinger equation. Figure 5 shows the values of $f_{1s,np}$ as function of screening parameter $\mu$, indicating a rapid decrease of $f_{1s,np}$ with increasing $\mu$.

The values of the absorption oscillator strengths for the three branches of the Balmer series are given in Table III up to $n=5$) for a number of Debye screening lengths. It is evident from this table that with decreasing $\delta$ the oscillator strengths of each Balmer series branch rapidly decrease.

The values of the absorption oscillator strengths for the $\Delta n=0$ transitions, $2s$-$2p$, $3s$-$3p$ and $3p$-$3d$, are given in Table IV for a number of Debye screening lengths. As expected, the oscillator strengths for these transitions increase with decreasing $\delta$. As function of the screening parameter $\mu$ they are shown in Fig. 6, together with the absorption oscillator strengths for the $4s$-$4p$, $4p$-$4d$, and $4d$-$4f$ transitions. We observe that with increasing $\mu$, the increase of $f_{n,l;n,l+1}$ is sharper for the larger $n$. Thus, already for relatively modest screenings with $\delta=20a_0$ the oscillator strengths $f_{4l;4,l+1}$ have values of 0.4–0.6, while the values of $f_{3l;3,l+1}$ are about 10 times smaller. The oscillator strength $f_{n,l;n,l+1}$ obtains its largest values when $\mu$ approaches the critical value $\mu_{n,l+1}$ of the upper state where $\omega_{n,l;n,l+1}$ gets also its largest values.

Figures 5 and 6 show (as well as Tables II–IV) that the absorption oscillator strengths for $\Delta n \neq 0$ and $\Delta n=0$ transitions are, roughly speaking, within the same order of magnitude for $n \leqslant 4$, with the difference that when $\mu$ increases the former decrease whereas the latter increase. For a given value of $\mu$, the oscillator strengths for $\Delta n \neq 0$ transitions decrease with increasing the principal quantum number of the upper state $n$, while for the $\Delta n=0$ transitions they increase with $n$. The scaled radiative transition probabilities $A_{n'l',nl}(\delta)$, Eq. (14), however, show a quite different picture regarding their magnitude for these two types of transitions. Figure 7 shows the $\mu$ dependence of the scaled radiative transition probabilities for the Lyman series $[np \rightarrow 1s$ panel (a)] and for the three branches of the Balmer series [panels (b), (c), and (d)] for $n' \leqslant 5$. In Fig. 8 we show the similar dependence of the $2p \rightarrow 2s$, $3p \rightarrow 3s$, $3d \rightarrow 3p$ [panel (a)] and $4p \rightarrow 4s$, $4d \rightarrow 4p$, $4f \rightarrow 4d$ [panel (b)] transitions. While the character of the $\mu$ dependence of $A_{n'l',nl}(\mu)$ for $\Delta n \neq 0$ and $\Delta n=0$ transitions remains the same as that for the corresponding absorption oscillator strengths, the magnitudes of scaled radiative transition probabilities for the $\Delta n \neq 0$ transitions are two to three orders larger than those for the $\Delta n=0$ transitions. This is a consequence of the additional $\omega^2_{nl,n'l'}(\delta)$ factor in the expression (14) for $A_{n'l',nl}(\delta)$ with respect to that for $f_{nl,n'l'}(\delta)$, Eq. (12), which for the $\Delta n \neq 0$ transitions is about two orders of magnitude larger than for the $\Delta n=0$ transitions (cf. Figs. 1 and 2).

In Figs. 7 and 8 we also show (by crosses) the values of transition probabilities from Ref. [3] for a number of $\mu$ values. The calculations in Ref. [3] were limited to the $n' \leqslant 3$ states only. The radial Schrödinger equation in Ref. [3] was solved by using the variational method with a Slater-type basis of trial functions. The values of transition probabilities of Ref. [3] differ from ours in the third significant digit only. It is to be noted in Figs. 7(b)–7(d) that the transition probabilities of the $nd \rightarrow 2p$ branch of the Balmer series are significantly larger than those for the other two branches.

In concluding this section we give the results for the radiative lifetimes $\tau_{nl}(Z,D)$ of excited $nl$ states of hydrogenlike ions in a Debye plasma for $n \leqslant 4$. These are defined by the relations

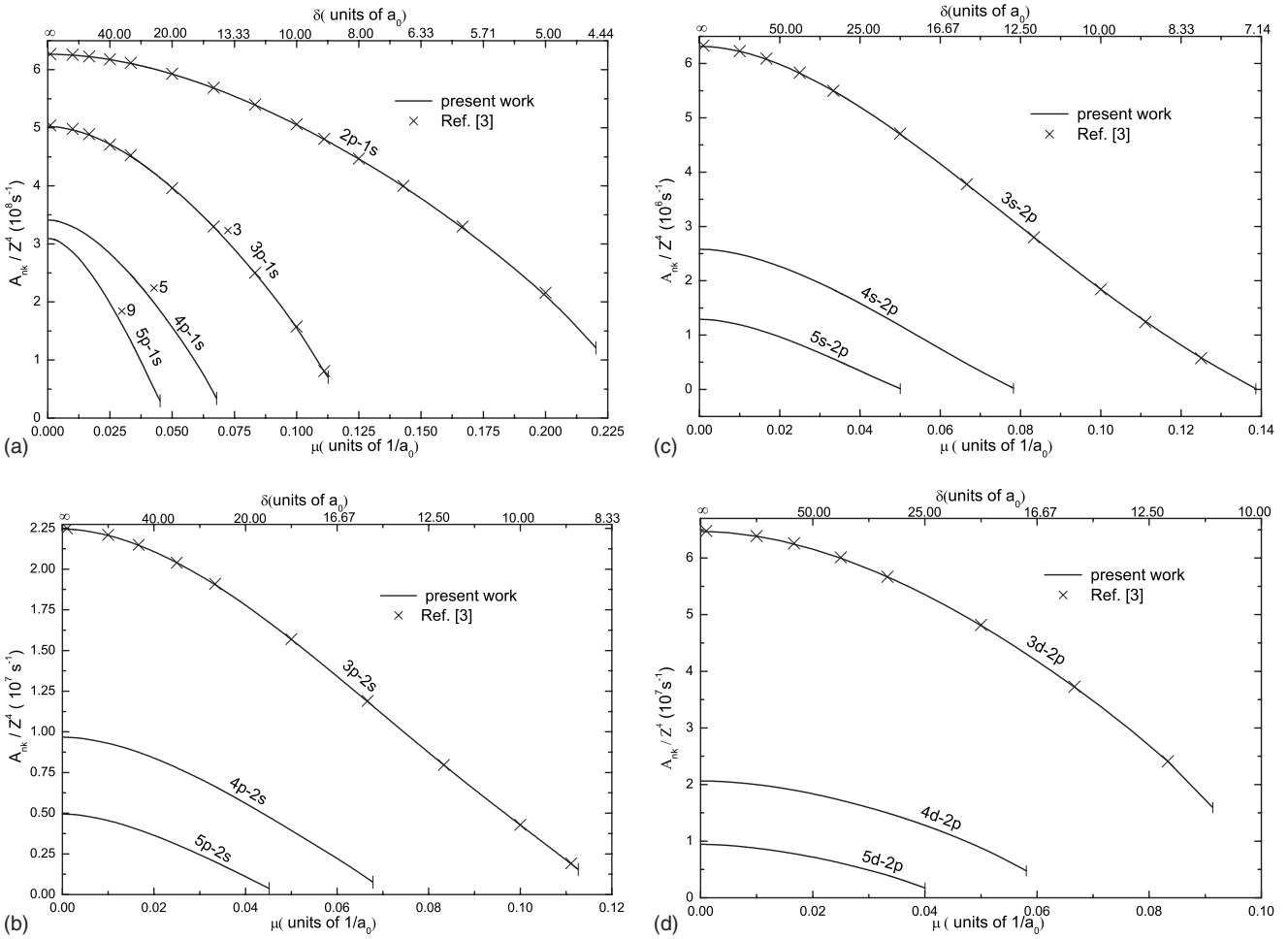


FIG. 7. Scaled radiative transition probabilities as function of screening parameter $\mu$. Panel (a), Lyman series; panels (b), (c), and (d), the three branches of the Balmer series for $n \leqslant 5$.

$$\tau_{nl}(Z,D) = Z^{-4}\tau_{nl}(\delta), \quad \tau_{nl}(\delta) = \left(\sum_k A_{nl,n_k l_k}(\delta)\right)^{-1}, \quad (15)$$

where $n_k \leqslant n$, and the summation runs over all dipole-allowed transitions. Figure 9 shows the scaled radiative lifetimes of $n \leqslant 4$ states as function of the screening parameter $\mu$. The lifetimes increase with increasing $\mu$, and for a given $l$ they increase with increasing $n$. The sharp increase of the lifetimes of the $3s$ and $4s$ states when $\mu$ approaches the corresponding critical values $\mu_{3s}$ and $\mu_{4s}$, respectively, is the result of the very small values of transition probabilities $A_{ns,n_k p}(\mu)$ near and at the critical points $\mu_{ns}$ [see Fig. 7(c)].

## IV. SPECTRAL LINE INTENSITIES AND SHIFTS

Under local thermodynamic equilibrium conditions, the spectral line intensity associated with the transition $|n'l'\rangle \rightarrow |nl\rangle$ in a hydrogenlike ion with charge $Z$ embedded in a Debye plasma with screening length $D$ is given by [19]

$$I_{n'l',nl}(Z,D) = \Delta E_{n'l',nl}(Z,D) A_{n'l',nl}(Z,D) N_{n'l'}, \quad (16)$$

$$N_{n'l'} = N_{1s}(2l'+1)\exp(-\Delta E_{n'l',1s}/T_e), \quad (17)$$

where $N_{n'l'}$ and $N_{1s}$ are the populations of the upper $|n'l'\rangle$ and the ground $|1s\rangle$ state, respectively, and $T_e$ is the plasma temperature expressed in energy units. As well known, the spectral lines in a plasma are subject to shift and broadening due to the thermal motion of the emitting particle or its interaction with the surrounding plasma particles. In the present study we shall consider only the thermal effects on the spectral lines described by the Doppler line profile function [19]

$$S(\omega) = \left(\frac{\ln 2}{\pi\Gamma^2}\right)^{1/2} \exp[-\ln 2(\omega-\omega_0)^2/\Gamma^2], \quad (18)$$

where $\omega_0 = \Delta E_{n'l',nl}(Z,D)$ and $\Gamma$ is the half-width of the line given by

$$\Gamma = [2\alpha^2 T_e(\ln 2)/M]^{1/2}\omega_0 \quad (19)$$

with $M$ being the mass of the emitting ion. The line intensity, normalized to the population of ground-state hydrogenlike ions $N_{1s}$, is now given by

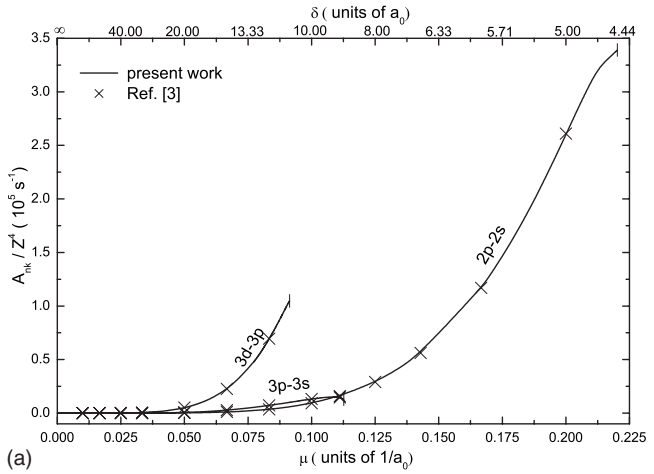


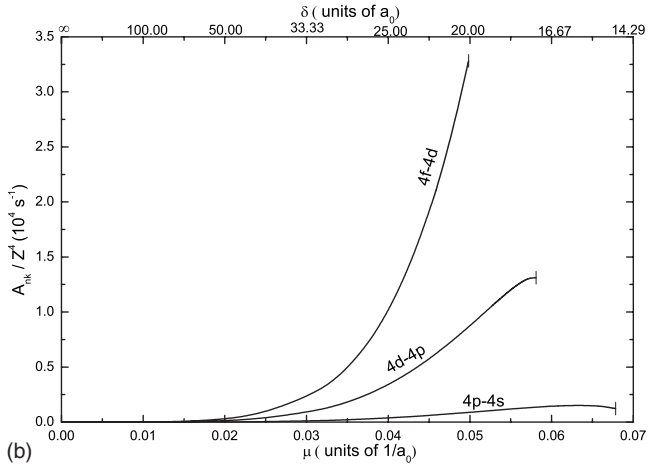


FIG. 8. Scaled radiative transition probabilities as function of screening parameter $\mu$. Panel (a), $2p \rightarrow 2s$, $3p \rightarrow 3s$, $3d \rightarrow 3p$; panel (b), $4p \rightarrow 4s$, $4d \rightarrow 4p$, $4f \rightarrow 4d$.

$$I_{n'l',nl}(Z,D)/N_{1s} = (2l'+1)\omega_0 A_{n'l',nl}(Z,D) \times \exp(-\Delta E_{n'l',1s}/T_e) S(\omega). \quad (20)$$

We note that $A_{n'l',nl}(Z,D) \propto \omega_0^2$ and, hence, the line intensity is proportional to $\omega_0^3$. The presence of the ion mass in the expression (19) for $\Gamma$ does not allow us to give the normalized line intensity in a scaled form with respect to $Z$. Therefore, we present the results for specific ions. However, the observed plasma effects on the spectral line properties have general character.

In Fig. 10 we show the reduced (by the population $N_{1s}$ of the ground state) intensities of Lyman-$\alpha$ [panel (a)] and $2p \rightarrow 2s$ line [panel (b)] in the H atom for a number of screening lengths $D$ and a fixed plasma temperature of 2024 eV. [We note that the half-width $\Gamma$ in the calculations of intensities in Fig. 10(b) was multiplied by a factor of 80 in order to make the width of these lines visible in the figure.] Figure 10(a) also shows the Lyman-$\alpha$ line when the interaction is unscreened. The plasma screening effects on the Lyman-$\alpha$ line are manifested in the decrease of its intensity and the redshift of its frequency when the Debye screening length decreases. The frequency redshift is, as mentioned earlier, the result of

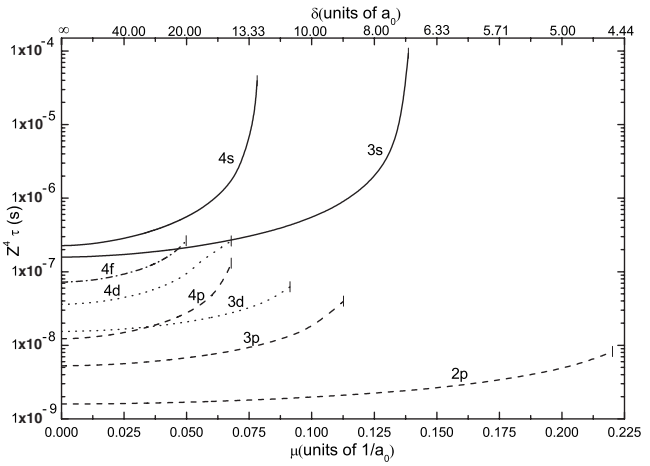


FIG. 9. Scaled radiative lifetimes of $n \leqslant 4$ states as function of the screening parameter $\mu$.

the decrease of the energy difference $\Delta E_{2p,1s}$ with decreasing $D$ (see Fig. 2), while the decrease of line intensity is due to the predominance of the $\omega_0^3$ factor in Eq. (20) and its decrease with decreasing $D$. The plasma screening effects on

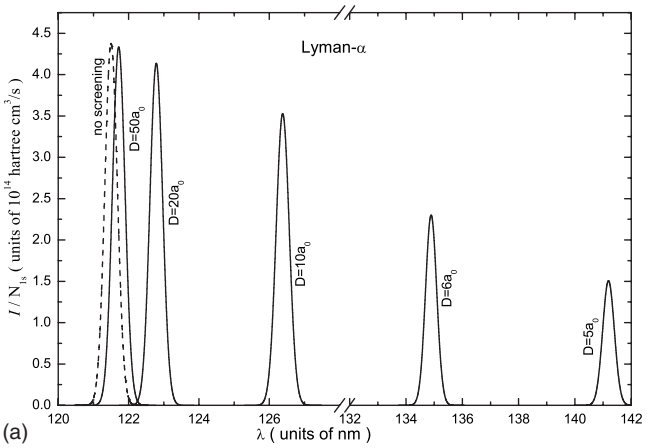


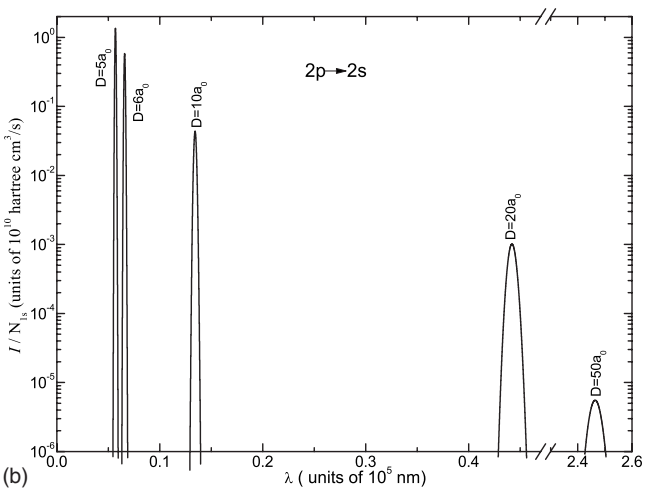


FIG. 10. Reduced intensities of hydrogen atom lines for a number of screening lengths $D$ and a fixed plasma temperature of 2024 eV. Panel (a), Lyman-$\alpha$; panel (b), the $2p \rightarrow 2s$ line (with the half-width enlarged 80 times for visibility).

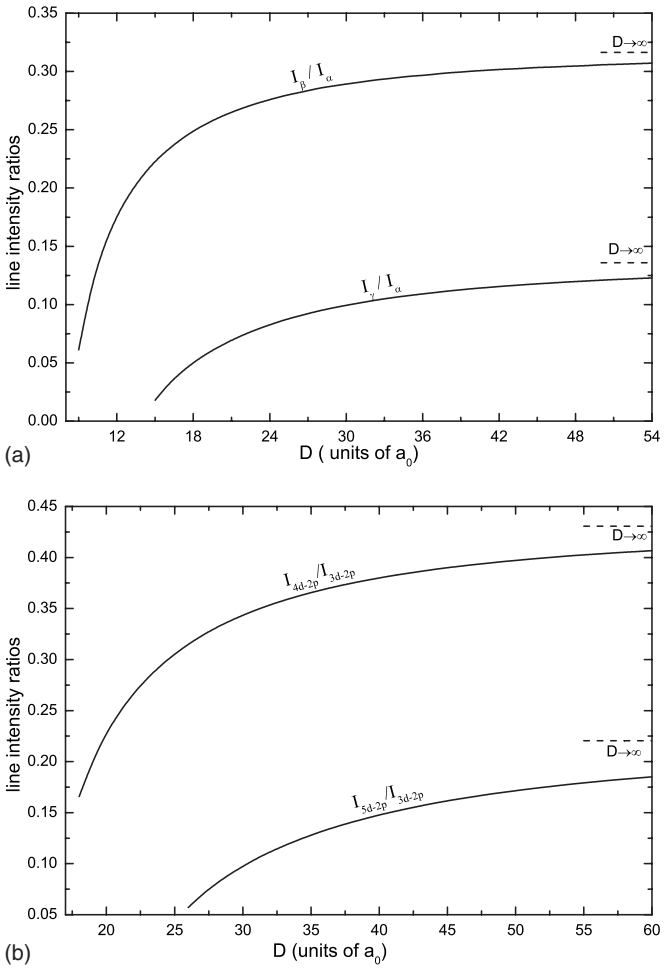


FIG. 11. Line intensity ratios of hydrogen atom for a fixed plasma temperature of 2024 eV as function of Debye screening length. Panel (a), $I_\beta/I_\alpha$ and $I_\gamma/I_\alpha$ of the Lyman series; panel (b), for the $nd \rightarrow 2p$ branch of the Balmer series.

the $2p \rightarrow 2s$ line are opposite to those on the Lyman-$\alpha$ line and result from the increase of $\Delta E_{2p,2s}$ with decreasing $D$. It is worthwhile to note that whereas in the considered interval of variation of $D$ the intensity of Lyman-$\alpha$ line changes by a factor of about 3, the intensity of $2p \rightarrow 2s$ line changes by more than five orders of magnitude. This is a consequence of the rapid decrease to zero when $D$ increases. It should also be noted that for a given value of $D$, the intensity of Lyman-$\alpha$ line is at least four orders of magnitude stronger than that of the $2p \rightarrow 2s$ line.

Of particular interest to plasma diagnostics are the intensity ratios of spectral lines within a given spectral series. In Fig. 11 we show the variation with the screening length of the line intensity ratios $I_\beta/I_\alpha$ and $I_\gamma/I_\alpha$ of the Lyman series [panel (a)] and the similar ratios of the lines of the $nd \rightarrow 2p$ branch of the Balmer series [panel (b)] of the hydrogen atom for a fixed plasma temperature of 2024 eV. For the small values of $D$ these ratios are rather small but they increase relatively rapidly towards their asymptotic values (of the unscreened Coulomb interaction) when $D$ increases.

It is important to emphasize that due to the successive exit of the $nl$-energy levels from the discrete to the continuum

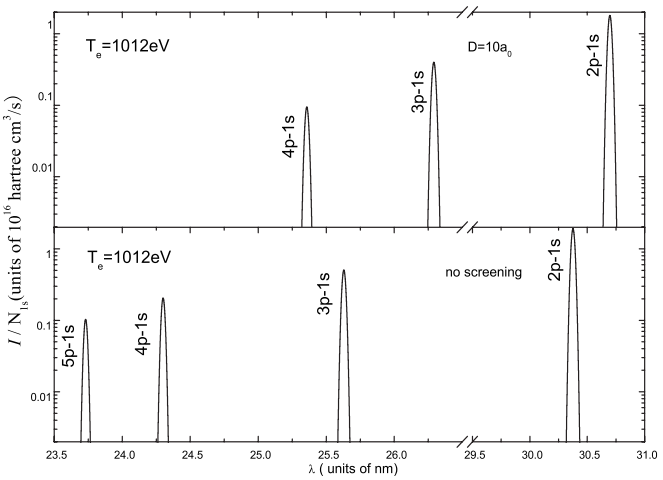


FIG. 12. Reduced intensities of Lyman series lines for the $He^+$ ion for $D=10a_0$ and $T_e=1012$ eV. The bottom panel shows the lines in the case of no interaction screening.

spectrum with decreasing the screening length, for a given value of $D$ the higher members of a given spectral series will not appear in the line spectrum. Thus, for $D=10a_0$ the state $4p$ of hydrogen atom and the state $5p$ of the $He^+$ ion already lie in the continuum (see Table I and the Lyman series of these one-electron systems contain only two and three lines, respectively. (The disappearance of high $nl$ terms from the spectral series is sometimes interpreted as "lowering of the continuum," or figuratively called "pressure ionization;" see, e.g., [1,2].) As we have mentioned in the Introduction, the reduction of Lyman series in dense plasmas to a finite number of lines has been experimentally observed both for H atoms [7,9,10] and other elements (Be and Al in [6], C in [8]).

In Figs. 12 and 13 we show, respectively, the reduced intensities of spectral lines of the Lyman series of $He^+$ and $C^{5+}$ ions for the fixed Debye screening length $D=10a_0$ and plasma temperature of 1012 eV. (For this value of $D$, the $9p$ state of $C^{5+}$ lies in the continuum.) In the bottom panels of these figures the corresponding lines in the unscreened case are also shown. The decrease of line intensities within the

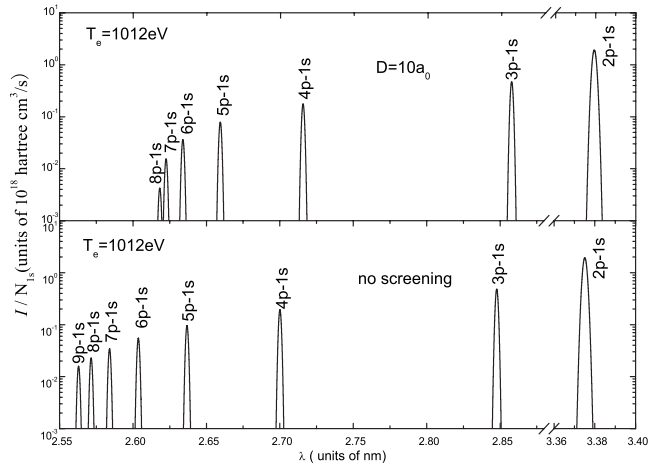


FIG. 13. Same as in Fig. 12, but for the $C^{5+}$ ion.

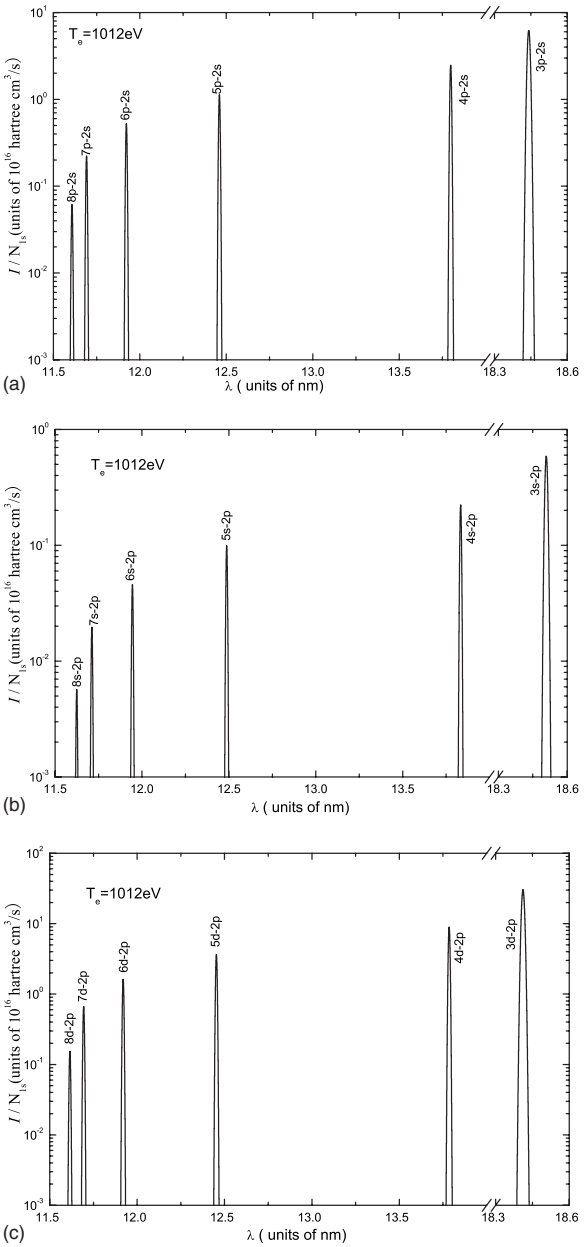


FIG. 14. Reduced line intensities of the three branches of Balmer series of $C^{5+}$ ion for $D=10a_0$ and $T_e=1012$ eV.

series with increasing the principal quantum number of the upper state is similar to that in the case of pure Coulomb interaction. Only the lines close to the termination of the series in the screened interaction case become significantly weaker with respect to the unscreened case (as illustrated by $7p$-$1s$ and $8p$-$1s$ lines in $C^{5+}$ in Fig. 13).

In Figs. 14(a)–14(c) the reduced intensities of spectral lines of the three branches of the Balmer series in the $C^{5+}$ ion are shown for $D=10a_0$ and $T_e=1012$ eV. The characteristic features of these line series are similar to those of the Lyman series in Fig. 13.

## V. CONCLUSIONS

In the present paper we have studied the spectral properties of bound-bound transitions in hydrogenlike ions in a Debye plasma, in which the interaction between charged particles is given by Eq. (1). The bound state energies and wave functions of hydrogenlike ions were obtained by solving the scaled radial Schrödinger equation for a wide range of values of the scaled Debye screening length, $\delta=ZD$, by the fourth-order symplectic integration method ensuring their high accuracy.

The plasma screening of the interaction potential is manifested in lifting the $l$ degeneracy of hydrogenic energy levels, decrease of the binding energies of $nl$ states when the screening length $\delta$ decreases, and in the decrease (increase) of energy differences for the states with $\Delta n \neq 0$ ($\Delta n=0$) when $\delta$ decreases. Due to the finiteness of the number of bound states in the potential (1), each $nl$-energy level enters the continuum at a certain value $\delta_{nl}$ of the scaled screening length. These changes in the energy spectrum of hydrogenlike ions in a Debye plasma strongly affect the characteristics of bound-bound transitions (oscillator strengths, radiative transition probabilities, radiative lifetimes) as well as the spectral lines associated with these transitions and their series. The lines associated with the $\Delta n \neq 0$ transitions are redshifted and their intensities decrease with decreasing $\delta$, while those for the $\Delta n=0$ transitions show opposite behavior. Due to the finite number of bound states in the hydrogenlike ion for any finite value of $\delta$, the number of lines within a given spectral series is always limited and decreases with decreasing $\delta$. When the state $n_0l_0$ of the series $nl \rightarrow n_0l_0 (n>n_0, l=l_0 \pm 1)$ enters the continuum, the entire series disappears from the spectrum.

## ACKNOWLEDGMENTS

One of us (R.K.J.) is grateful to the Institute of Applied Physics and Computational Mathematics, Beijing, for the warm hospitality during the period when this work was performed. This work was partly supported by the National Natural Science Foundation of China (Grants No. 10604011, No. 10571074, 10734140 and No. 10574018).

[1] D. Salzman, *Atomic Physics in Hot Plasmas* (Oxford University Press, Oxford, 1998).
[2] M. S. Murillo and J. C. Weisheit, Phys. Rep. **302**, 1 (1998).
[3] K. M. Roussel and R. F. O'Connell, Phys. Rev. A **9**, 52 (1974).
[4] J. C. Weisheit and B. W. Shore, Astrophys. J. **194**, 519 (1974).
[5] F. E. Hohne and R. Zimmermann, J. Phys. B **15**, 2551 (1982).
[6] K. Eidmann, W. Schwanda, I. B. Földers, R. Sigel, and G. D. Tsakiris, J. Quant. Spectrosc. Radiat. Transf. **51**, 77 (1994).
[7] St. Böddeker, S. Günter, A. Könies, L. Hitzschke, and H.-J. Kunze, Phys. Rev. E **47**, 2785 (1993).
[8] M. Nantel, G. Ma, S. Gu, C. Y. Côté, J. Itatani, and D. Umstadter, Phys. Rev. Lett. **80**, 4442 (1998).

[9] H. Nozato, S. Morita, M. Goto, Y. Takase, A. Ejiri, T. Amano, K. Tanaka, and S. Inakagi, Phys. Plasmas **11**, 1920 (2004).
[10] M. Goto, R. Sakamoto, and S. Morita, Plasma Phys. Controlled Fusion **49**, 1163 (2007).
[11] P. Chandhury and S. P. Bhattacharyya, Chem. Phys. Lett. **296**, 51 (1998).
[12] C. Stubbins, Phys. Rev. A **48**, 220 (1993).
[13] F. J. Rogers, H. C. Graboske, and D. J. Harwood, Phys. Rev. A **1**, 1577 (1970).
[14] E. Forest and R. D. Ruth, Physica D **43**, 105 (1990); H. Yoshida, Phys. Lett. A **150**, 262 (1990).
[15] X. S. Liu, X. Y. Liu, Z. Y. Zhou, P. Z. Ling, and S. F. Pan, Int. J. Quantum Chem. **79**, 343 (2000).
[16] F. Herman and S. Skillman, *Atomic Structure Calculations* (Prentice-Hall, Englewood Cliffs, NJ, 1963).
[17] L. D. Landau and E. M. Lifshitz, *Quantum Mechanics: Non-Relativistic Theory* (Pergamon, London, 1958).
[18] H. A. Bethe and E. E. Salpeter, *Quantum Mechanics of One- and Two-Electron Atoms* (Academic, New York, 1957).
[19] R. W. Cowan, *The Theory of Atomic Structure and Spectra* (University of California Press, Berkeley, 1981).